International Journal of Heat and Mass Transfer 53 (2010) 4002–4016

Contents lists available at ScienceDirect

International Journal of Heat and Mass Transfer

journal homepage: www.elsevier.com/locate/ijhmt

Analytical heat diffusion models for different micro-channel heat sink cross-sectional geometries

Sung-Min Kim, Issam Mudawar *

Boiling and Two-Phase Flow Laboratory (BTPFL), Purdue University International Electronic Cooling Alliance (PUIECA), Mechanical Engineering Building, 585 Purdue Mall West Lafayette, IN 47907-2088, USA

ARTICLE INFO

Article history:
Received 20 November 2009
Received in revised form 10 April 2010
Accepted 10 April 2010
Available online 10 June 2010

Keywords:
Analytical heat diffusion model
Micro-channel heat sink
Flow boiling

ABSTRACT

This study explores heat diffusion effects in micro-channel heat sinks intended for electronic cooling applications. Detailed analytical models are constructed for heat sinks having micro-channels with rectangular, inverse trapezoidal, triangular, trapezoidal, and diamond-shaped cross sections. Solutions are presented for both monolithic heat sinks and heat sinks with perfectly insulating cover plates. The analytical results are compared to detailed two-dimensional numerical models of the same cross-sections over a broad range of cover plate thermal conductivities for different micro-channel aspect ratios, fin spacings and Biot numbers. These comparisons show the analytical models provide accurate predictions for Biot numbers of practical interest. This study proves the analytical models are very effective tools for the design and thermal resistance prediction of micro-channel heat sinks found in electronic cooling applications.

1. Introduction

The past two decades have witnessed intense interest among researchers in the use of micro-channel heat sinks, which has been spurred by such unique attributes as compactness, high power dissipation to volume ratio, and small coolant inventory. Because of the relative simplicity of fabricating rectangular micro-channels, the vast majority of these studies involve rectangular cross-sections. However, an increasing number of single-phase and two-phase heat transfer studies is focusing on sinks having non-rectangular cross-sections such as triangular [1–3], trapezoidal [4,5], and diamond-shaped [6], citing thermal benefits to these cross-sections related to heat diffusion effects and bubble nucleation in sharp corners. Since the heat sink is typically designed to conduct heat away from a high-heat-flux electronic or power device that is attached directly to the heat sink, heat diffusion within the heat sink is responsible for an important thermal resistance between the device's surface and the coolant. Unfortunately, published work describing heat diffusion effects in heat sinks having non-rectangular micro-channels is quite sparse.

In case of a monolithic micro-channel heat sink, the local heat transfer coefficient at an axial location along the micro-channel can be determined from the relation

$$h = \frac{q''}{T_w - T_f}, \tag{1}$$

where q'', T_w, and T_f are the average heat flux along the micro-channel wall, the average channel wall temperature, and the bulk fluid temperature, respectively. However, as direct temperature measurement of the micro-channel perimeter is not practical, the fin analysis method is often used in experimental studies (see [7,8]) to evaluate the local heat transfer coefficient. For example, in case of a heat sink with rectangular micro-channels and three-sided heating (*i.e.*, with a perfectly insulating top cover plate), applying the fin analysis method to the system illustrated in Fig. 1a yields [7]

$$h = \frac{q''_{eff}(2H_{ch} + W_{ch})}{(T_{w,b} - T_f)(2\eta H_{ch} + W_{ch})} = \frac{q''_{base}(W_{ch} + W_s)}{(T_{w,b} - T_f)(2\eta H_{ch} + W_{ch})}, \tag{2}$$

where q''_{base} is the device heat flux, and the fin efficiency and fin parameter are defined as [9]

$$\eta = \frac{\tanh(mH_{ch})}{mH_{ch}} \quad \text{and} \quad m = \sqrt{\frac{2h}{kW_s}}, \tag{3}$$

respectively. In Eq. (2), $T_{w,b}$ represents the temperature corresponding to the entire bottom plane of the micro-channels, which is assumed uniform in Refs. [7,8]. This temperature can be determined from the temperature T_{base} of the device by assuming one-dimensional heat conduction between the plane of the device and the bottom plane of the micro-channels.

$$T_{w,b} = T_{base} - \frac{q''_{base}H_b}{k}. \tag{4}$$

The one-dimensional fin analysis method is a convenient and accurate means to determining the heat transfer coefficient in a micro-channel heat sink provided the Biot number, based on half-width of the solid wall separating channels for the rectangular cross-section is sufficiently small [10,11]. As will be shown later in

* Corresponding author. Tel.: +1 765 494 5705; fax: +1 765 494 0539.
E-mail address: mudawar@ecn.purdue.edu (I. Mudawar).

0017-9310/$ - see front matter © 2010 Elsevier Ltd. All rights reserved.
doi:10.1016/j.ijheatmasstransfer.2010.05.019

Nomenclature

a	coefficient in Eq. (19)
A_c	cross-sectional area of fin
A_s	surface area of fin exposed to convection
AR	aspect ratio of micro-channel, H_{ch}/W_{ch}
b	fin length
Bi	biot number, $hW_s/2k$
C_1, C_2	coefficients in fin equation
d	fin length
h	heat transfer coefficient
H_b	distance from bottom of heat sink to bottom of micro-channel
H_c	height of cover plate
H_{ch}	micro-channel height
I_n	Nth-order Bessel function of first kind
k	thermal conductivity of heat sink solid
k_c	thermal conductivity of cover plate
K_n	Nth-order Bessel function of second kind
m	fin parameter
Q	heat transfer rate per unit length
q'	heat transfer rate per unit length
q''	heat flux
q''_{base}	heat flux based on base area of heat sink; device heat flux
q''_{eff}	heat flux based on heated perimeter of micro-channel
T	temperature
T_{base}	temperature of heat sink base; device temperature
$T_{w,b}$	mean temperature of bottom plane of micro-channels
$T_{w,t}$	mean temperature of top plane of micro-channels
W_{ch}	micro-channel width
W_s	width of solid wall separating micro-channels
$W_{s,e}$	width of endwall
x	coordinate

Greek symbols

δ_b	fin thickness at base
ξ_1, ξ_2, ξ_3, ξ_4	parameters in temperature functions
η	fin efficiency
θ	temperature difference in fin equation

Subscripts

1	micro-channel left wall
2	fin tip; tip of solid wall separating micro-channels
2a	micro-channel top wall
A	analytical
b	micro-channel bottom wall
$base$	heat sink base
c	cover plate
ch	micro-channel
f	bulk fluid
fin	fin base; base of solid wall separating micro-channels
N	numerical
t	micro-channel top wall
tip	adiabatic fin tip for diamond channel
w	micro-channel wall

this study, the one-dimensional approach is valid for most micro-channel experiments with rectangular micro-channels because $Bi << 0.1$. However, it should be emphasized that Eq. (2) is valid only for three-sided heated rectangular micro-channels, *i.e.*, when the cover plate is perfectly insulating.

The objective of this study is to derive one-dimensional analytical solutions for heat diffusion in micro-channel heat sinks having rectangular, inverse trapezoidal, triangular, trapezoidal, and diamond-shaped micro-channel cross-sections as illustrated in Fig. 1. Unlike earlier published studies, the effect of the thermal conductivity of the cover plate will be taken into consideration. Excepting the diamond-shaped cross-section, two sets of exact solutions are presented for each cross section: monolithic heat sinks ($k_c = k$), and heat sinks with perfectly insulating cover plates ($k_c = 0$). To validate the analytical solutions, a parametric study of channel aspect ratio, fin spacing and Biot number is performed, and the analytical predictions are compared to numerical solutions of the two-dimensional heat diffusion equation for the different cross-sectional geometries.

2. Longitudinal fin analyses

Fig. 2 illustrates the schematic diagrams for three basic longitudinal fins with rectangular, trapezoidal, and inverse trapezoidal profiles that are used to derive the diffusion models for the heat sink micro-channel geometries illustrated in Fig. 1. It should be emphasized that, while certain solutions have been published for some of these fin profiles under boundary conditions of interest to micro-channel heat sink geometries, solutions are not available for others and are therefore derived in detail in the present paper. In the following, solutions to all relevant boundary conditions will be presented, with each solution obtained from prior sources carefully indicated as such.

The following conventional assumptions are made in the one-dimensional fin analysis [12,13]:

1. The heat conduction in the fin is steady and one-dimensional along the x-direction.
2. The fin material is homogeneous and isotropic.
3. The thermal conductivity of the fin is constant and uniform.
4. The heat exchange between the fin and the surrounding fluid is solely by convection along the fin surface.
5. There is no heat generation within the fin itself.
6. The heat transfer coefficient and the temperature of the surrounding fluid are constant and uniform.

Applying energy conservation to the differential elements shown in Fig. 2, the governing second-order ordinary differential equation for one-dimensional steady-state temperature distribution can be derived as follows [9]:

$$\frac{d^2T(x)}{dx^2} + \left(\frac{1}{A_c}\frac{dA_c(x)}{dx}\right)\frac{dT(x)}{dx} - \left(\frac{1}{A_c}\frac{h}{k}\frac{dA_s(x)}{dx}\right)(T(x) - T_f) = 0, \quad (5)$$

where A_c and A_s are the cross-sectional area and the surface area of the fin exposed to convection, respectively.

2.1. Rectangular fin

For the rectangular fin, A_c is constant and Eq. (5) can be written as

$$\frac{d^2\theta}{dx^2} - m^2\theta = 0. \quad (6)$$

Eq. (6) has the solution

$$\theta(x) = C_1 exp(mx) + C_2 exp(-mx). \quad (7)$$

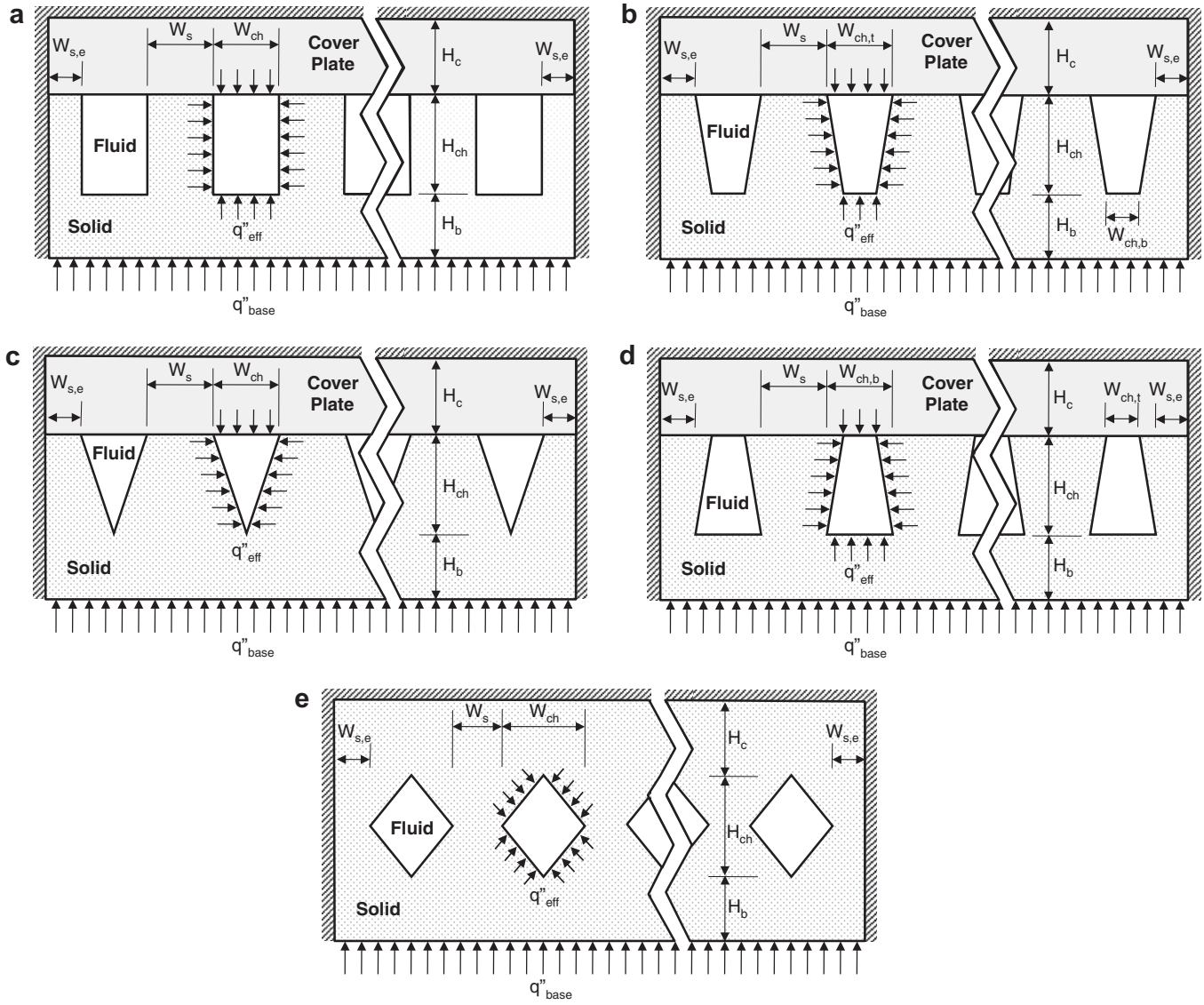

Fig. 1. Schematic diagrams of micro-channel heat sinks with (a) rectangular, (b) inverse-trapezoidal, (c) triangular, (d) trapezoidal, and (e) diamond-shaped cross-sections.

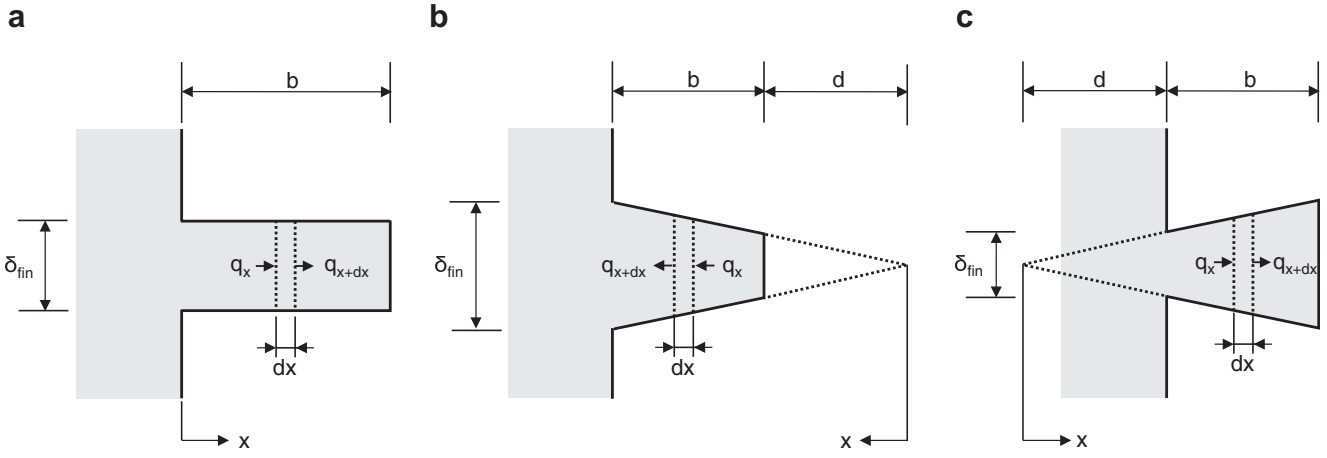

Fig. 2. Schematic diagrams of (a) rectangular, (b) trapezoidal and (c) inverse trapezoidal fins.

where

$$\theta(x) = T(x) - T_f \quad \text{and } m = \sqrt{\frac{2h}{k\delta_{fin}}}. \tag{8}$$

The above equation is subjected to the following boundary conditions that are of interest to micro-channel heat-sink modeling.

2.1.1. Constant base temperature and adiabatic tip

$$\theta(0) = \theta_{fin} \tag{9}$$

and

$$\left.\frac{d\theta}{dx}\right|_{x=b} = 0. \tag{10}$$

The exact solution of Eq. (6) with boundary conditions (9) and (10) gives the following temperature distribution along the fin,

$$\frac{\theta(x)}{\theta_{fin}} = \frac{cosh(m(b-x))}{cosh(mb)}, \tag{11}$$

from which the heat transfer rate at the fin base can be obtained as

$$q'_{fin} = -kA'_c \left.\frac{d\theta}{dx}\right|_{x=0} = k\delta_{fin}\theta_{fin} m \tanh(mb). \tag{12}$$

2.1.2. Constant base temperature and prescribed tip temperature

$$\theta(0) = \theta_{fin} \tag{13}$$

and

$$\theta(b) = \theta_2. \tag{14}$$

The solution to Eq. (6) with boundary conditions (13) and (14) is given by

$$\frac{\theta(x)}{\theta_{fin}} = \frac{(\theta_2/\theta_{fin})\sinh(mx) + \sinh(m(b-x))}{\sinh(mb)} \tag{15}$$

and the heat transfer rates at the fin base and at the fin tip are given, respectively, as

$$q'_{fin} = -kA'_c \left.\frac{d\theta}{dx}\right|_{x=0} = k\delta_{fin} m \frac{cosh(mb)\theta_{fin} - \theta_2}{sinh(mb)} \tag{16}$$

and

$$q'_2 = -kA'_c \left.\frac{d\theta}{dx}\right|_{x=b} = k\delta_{fin} m \frac{\theta_{fin} - \theta_2\cosh(mb)}{sinh(mb)}. \tag{17}$$

The same results of Eqs. (11), (12) and (15)–(17) are represented in [14] as elements of linear transformations.

2.2. Trapezoidal fin

Similar to the solution procedure for a rectangular fin, the governing Eq. (5) may be expressed as

$$\frac{d^2\theta}{dx^2} + \frac{1}{x}\frac{d\theta}{dx} - m^2 a\frac{\theta}{x} = 0, \tag{18}$$

where

$$m = \sqrt{\frac{2h}{k\delta_{fin}}} \quad \text{and } a = \sqrt{\frac{\delta_{fin}^2}{4} + (b+d)^2}. \tag{19}$$

The exact solution for the above second-order ordinary differential equation can be written in the form of modified Bessel functions [14].

$$\theta(x) = C_1 I_0\left(2m\sqrt{ax}\right) + C_2 K_0\left(2m\sqrt{ax}\right), \tag{20}$$

where I_0 and K_0 are modified, zero-order Bessel functions of the first and second kinds, respectively. Eq. (20) is subjected to the following boundary conditions.

2.2.1. Constant base temperature and adiabatic tip

$$\theta(b+d) = \theta_{fin}, \tag{21}$$

$$\left.\frac{d\theta}{dx}\right|_{x=d} = 0. \tag{22}$$

The exact solution of Eq. (18) with boundary conditions (21) and (22) gives the following temperature distribution along the fin.

$$\frac{\theta(x)}{\theta_{fin}} = \frac{I_0(2m\sqrt{ax})K_1\left(2m\sqrt{ad}\right) + K_0(2m\sqrt{ax})I_1\left(2m\sqrt{ad}\right)}{I_0\left(2m\sqrt{a(b+d)}\right)K_1\left(2m\sqrt{ad}\right) + K_0\left(2m\sqrt{a(b+d)}\right)I_1\left(2m\sqrt{ad}\right)}, \tag{23}$$

where I_n and K_n are modified, nth-order Bessel functions of the first and second kinds, respectively. The heat transfer rate at the fin base is given by

$$q'_{fin} = k\delta_{fin}\theta_{fin} m\sqrt{\frac{a}{b+d}} \times \frac{I_1\left(2m\sqrt{a(b+d)}\right)K_1\left(2m\sqrt{ad}\right) - K_1\left(2m\sqrt{a(b+d)}\right)I_1\left(2m\sqrt{ad}\right)}{I_0\left(2m\sqrt{a(b+d)}\right)K_1\left(2m\sqrt{ad}\right) + K_0\left(2m\sqrt{a(b+d)}\right)I_1\left(2m\sqrt{ad}\right)}. \tag{24}$$

It should be noted that similar expressions to Eqs. (23) and (24) are found in Bejan and Kraus [15], in which dA_s/dx in Eq. (5) is assumed equal to $2L$, where the fin thickness is small compared to its height. Although it is mentioned that this assumption is valid for most practical thin fins [13], the following general expression from [14,16] is used for more accurate results.

$$\frac{dA_s}{dx} = 2\sqrt{1 + \left(\frac{dy}{dx}\right)^2} = \frac{\sqrt{\delta_{fin}^2 + 4(b+d)^2}}{b+d}. \tag{25}$$

2.2.2. Constant base temperature and prescribed tip temperature

$$\theta(b+d) = \theta_{fin} \tag{26}$$

and

$$\theta(d) = \theta_2. \tag{27}$$

The temperature distribution and the heat transfer rates at the fin base and the fin tip with boundary conditions (26) and (27) are given, respectively, as follows:

$$\theta(x) = \frac{\left[K_0\left(2m\sqrt{ad}\right)\theta_{fin} - K_0\left(2m\sqrt{a(b+d)}\right)\theta_2\right]I_0(2m\sqrt{ax}) + \left[I_0\left(2m\sqrt{a(b+d)}\right)\theta_2 - I_0\left(2m\sqrt{ad}\right)\theta_{fin}\right]K_0(2m\sqrt{ax})}{I_0\left(2m\sqrt{a(b+d)}\right)K_0\left(2m\sqrt{ad}\right) - K_0\left(2m\sqrt{a(b+d)}\right)I_0\left(2m\sqrt{ad}\right)}, \tag{28}$$

$$q'_{fin} = k\delta_{fin} m\sqrt{\frac{a}{b+d}} \frac{\left[I_1\left(2m\sqrt{a(b+d)}\right)K_0\left(2m\sqrt{ad}\right) + K_1\left(2m\sqrt{a(b+d)}\right)I_0\left(2m\sqrt{ad}\right)\right]\theta_{fin} - \frac{\theta_2}{2m\sqrt{a(b+d)}}}{I_0\left(2m\sqrt{a(b+d)}\right)K_0\left(2m\sqrt{ad}\right) - K_0\left(2m\sqrt{a(b+d)}\right)I_0\left(2m\sqrt{ad}\right)} \tag{29}$$

and

$$q'_2 = k\delta_{fin} m \frac{\sqrt{ad}}{b+d} \frac{\frac{\theta_{fin}}{2m\sqrt{ad}} - \left[I_1\left(2m\sqrt{ad}\right)K_0\left(2m\sqrt{a(b+d)}\right) + K_1\left(2m\sqrt{ad}\right)I_0\left(2m\sqrt{a(b+d)}\right)\right]\theta_2}{I_0\left(2m\sqrt{a(b+d)}\right)K_0\left(2m\sqrt{ad}\right) - K_0\left(2m\sqrt{a(b+d)}\right)I_0\left(2m\sqrt{ad}\right)}. \tag{30}$$

The same results of Eqs. (23), (24) and (28)–(30) are represented in [14] as elements of linear transformations.

2.3. Inverse trapezoidal fin

The governing Eq. (5) can be written as follows:

$$\frac{d^2\theta}{dx^2} + \frac{1}{x}\frac{d\theta}{dx} - m^2 a\frac{\theta}{x} = 0, \tag{31}$$

where

$$m = \sqrt{\frac{2h}{k\delta_{fin}}} \quad \text{and} \quad a = \sqrt{\frac{\delta_{fin}^2}{4} + d^2}. \tag{32}$$

The general solution to Eq. (31) is given by [14]

$$\theta(x) = C_1 I_0\left(2m\sqrt{ax}\right) + C_2 K_0\left(2m\sqrt{ax}\right). \tag{33}$$

The above equation is subjected to the following boundary conditions.

2.3.1. Constant base temperature and adiabatic tip

$$\theta(d) = \theta_{fin} \tag{34}$$

and

$$\left.\frac{d\theta}{dx}\right|_{x=b+d} = 0 \tag{35}$$

The temperature distribution, and the heat transfer rate at the fin base with boundary conditions (34) and (35) are given, respectively, by

$$\frac{\theta(x)}{\theta_{fin}} = \frac{I_0(2m\sqrt{ax})K_1\left(2m\sqrt{a(b+d)}\right) + K_0(2m\sqrt{ax})I_1\left(2m\sqrt{a(b+d)}\right)}{I_0\left(2m\sqrt{ad}\right)K_1\left(2m\sqrt{a(b+d)}\right) + K_0\left(2m\sqrt{ad}\right)I_1\left(2m\sqrt{a(b+d)}\right)} \tag{36}$$

and

$$q'_{fin} = k\delta_{fin}\theta_{fin} m\sqrt{\frac{a}{d}} \times \frac{I_1\left(2m\sqrt{a(b+d)}\right)K_1\left(2m\sqrt{ad}\right) - K_1\left(2m\sqrt{a(b+d)}\right)I_1\left(2m\sqrt{ad}\right)}{I_0\left(2m\sqrt{ad}\right)K_1\left(2m\sqrt{a(b+d)}\right) + K_0\left(2m\sqrt{ad}\right)I_1\left(2m\sqrt{a(b+d)}\right)}. \tag{37}$$

2.3.2. Constant base temperature and prescribed tip temperature

$$\theta(d) = \theta_{fin} \tag{38}$$

and

$$\theta(b+d) = \theta_2. \tag{39}$$

The temperature distribution, and the heat transfer rates at the fin base and the fin tip with boundary conditions (38) and (39) are given, respectively, as

$$\theta(x) = \frac{\left[K_0\left(2m\sqrt{ad}\right)\theta_2 - K_0\left(2m\sqrt{a(b+d)}\right)\theta_{fin}\right]I_0(2m\sqrt{ax}) + \left[I_0\left(2m\sqrt{a(b+d)}\right)\theta_{fin} - I_0\left(2m\sqrt{ad}\right)\theta_2\right]K_0(2m\sqrt{ax})}{I_0\left(2m\sqrt{a(b+d)}\right)K_0\left(2m\sqrt{ad}\right) - K_0\left(2m\sqrt{a(b+d)}\right)I_0\left(2m\sqrt{ad}\right)}, \tag{40}$$

$$q'_{fin} = k\delta_{fin} m\sqrt{\frac{a}{d}} \frac{\left[I_1\left(2m\sqrt{ad}\right)K_0\left(2m\sqrt{a(b+d)}\right) + K_1\left(2m\sqrt{ad}\right)I_0\left(2m\sqrt{a(b+d)}\right)\right]\theta_{fin} - \frac{\theta_2}{2m\sqrt{ad}}}{I_0\left(2m\sqrt{a(b+d)}\right)K_0\left(2m\sqrt{ad}\right) - K_0\left(2m\sqrt{a(b+d)}\right)I_0\left(2m\sqrt{ad}\right)} \tag{41}$$

and

$$q'_2 = k\delta_{fin} m \frac{\sqrt{a(b+d)}}{d} \frac{\frac{\theta_{fin}}{2m\sqrt{a(b+d)}} - \left[I_1\left(2m\sqrt{a(b+d)}\right)K_0\left(2m\sqrt{ad}\right) + K_1(2m\sqrt{a(b+d)})I_0\left(2m\sqrt{ad}\right)\right]\theta_2}{I_0(2m\sqrt{a(b+d)})K_0\left(2m\sqrt{ad}\right) - K_0\left(2m\sqrt{a(b+d)}\right)I_0\left(2m\sqrt{ad}\right)}. \tag{42}$$

3. Micro-channel heat sinks

To obtain exact solutions for heat diffusion in the micro-channel heat sinks, the following additional assumptions are made based on the unit cells shown in Fig. 3 (see also Fig. 1):

1. The top surface of the cover plate is perfectly insulated.
2. In case of rectangular, inverse trapezoidal, and trapezoidal channels, the temperature of the fin base is the same as that of the micro-channel bottom wall, *i.e.*, $T_{fin} = T_b$.
3. In case of $k_c = k$ (monolithic heat sink), the temperature of the fin tip is the same as that of the micro-channel top wall, *i.e.*, $T_2 = T_{2a}$.
4. The effective heat flux, q''_{eff}, is averaged over the heated perimeter of the micro-channel. The heated perimeter consists of the entire wetted perimeter of the micro-channel, or, for the case of a perfectly insulating cover plate, the micro-channel perimeter minus the portion in contact with the cover plate.
5. The endwall width of the micro-channel heat sink is equal to the solid sidewall's half-width, *i.e.*, $W_{s,e} = 0.5W_s$.

3.1. Rectangular cross-section

The heat transfer rate at fin base can be obtained from the following energy balance for the micro-channel unit cell shown in Fig. 3a,

$$Q_{base} = Q_b + Q_{fin} = Q_b + Q_1 + Q_2 \ [\mathrm{W/m}]. \tag{43}$$

The heat transfer rate at the micro-channel bottom wall is given by

$$Q_b = hW_{ch}(T_{w,b} - T_f). \tag{44}$$

Introducing Eqs. (16) and (17) for the rectangular fin, the heat transfer rates at the fin base and the fin tip for the micro-channel unit cell can be written, respectively, as

$$Q_{fin} = \sqrt{2hkW_s}\frac{(T_{w,b} - T_f)\cosh(mH_{ch}) - (T_{w,t} - T_f)}{\sinh(mH_{ch})} \tag{45}$$

and

$$Q_2 = \sqrt{2hkW_s}\frac{(T_{w,b} - T_f) - (T_{w,t} - T_f)\cosh(mH_{ch})}{\sinh(mH_{ch})}, \tag{46}$$

where

$$m = \sqrt{\frac{2h}{kW_s}}. \tag{47}$$

By neglecting heat loss from the top of the cover plate, applying an energy balance to the cover plate gives

$$Q_{2a} = hW_{ch}(T_{w,t} - T_f) = Q_2. \tag{48}$$

This procedure yields the following expression for tip temperature,

$$T_{w,t} = T_f + \frac{\sqrt{2hkW_s}(T_{w,b} - T_f)}{hW_{ch}\sinh(mH_{ch}) + \sqrt{2hkW_s}\cosh(mH_{ch})}. \tag{49}$$

Applying an energy balance to the micro-channel heat sink shown in Fig. 1a yields

$$q''_{eff}(2H_{ch} + 2W_{ch}) = q''_{base}(W_s + W_{ch}) = Q_{fin} + Q_b. \tag{50}$$

It may be noted that the heat influx to the micro-channel can be expressed in terms of the effective heat flux or the base heat flux, as originally defined by Qu and Mudawar [7]. In the present study, the effective heat flux, q''_{eff}, and the base heat flux, q''_{base}, are defined as the mean heat flux based on the channel perimeter subjected to heating, and the heat flux based on heat sink base area, respectively, as illustrated in Fig. 3. In case of a perfectly insulating cover plate ($k_c = 0$), q''_{eff} has a zero value at the surface adjoining the cover plate, and is uniform over the other surfaces. For example, in the case of the rectangular micro-channel with insulating cover plate, q''_{eff} is assigned a value that is averaged over the three heating walls. If the base heat flux, q''_{base}, and the base temperature, $T_{w,b}$,

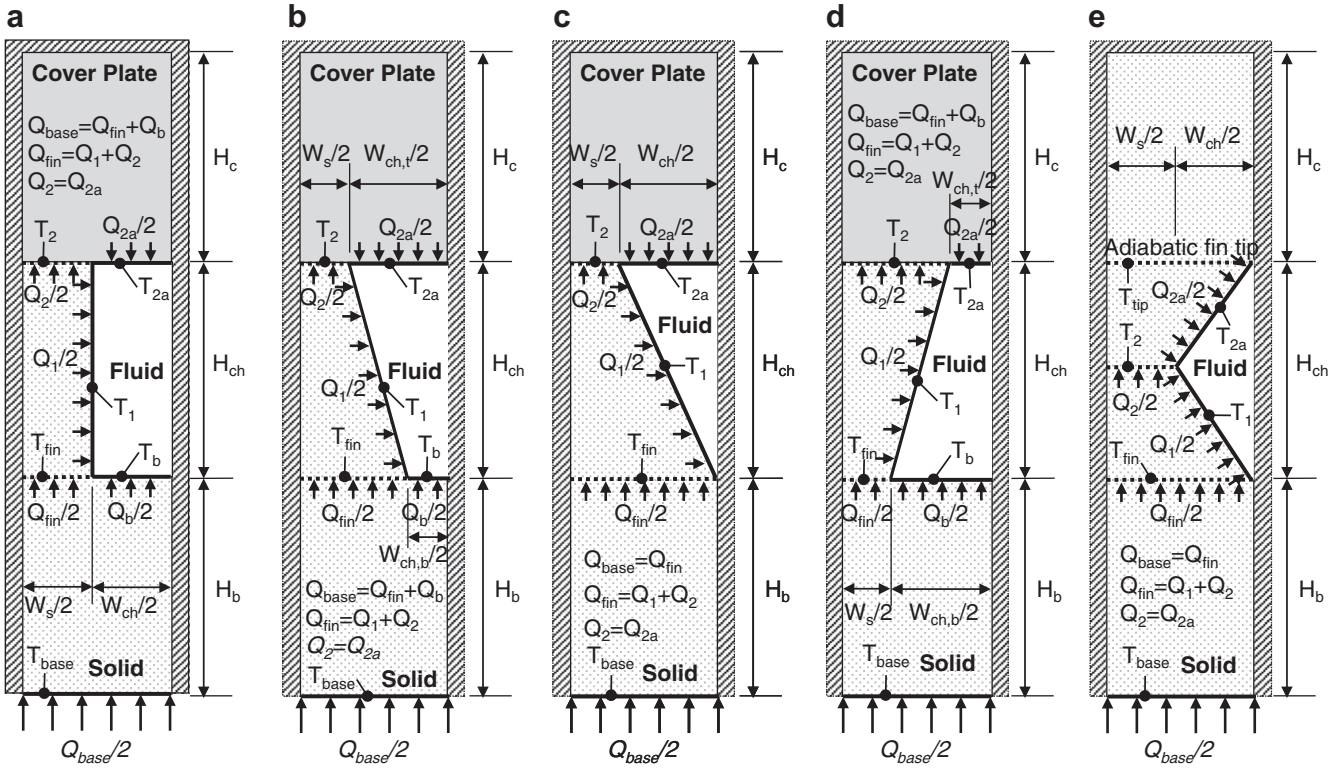

Fig. 3. Heat sink unit cells with: (a) rectangular, (b) inverse trapezoidal, (c) triangular, (d) trapezoidal, and (e) diamond-shaped micro-channel cross-sections.

are available from the actual device or measured from experiment, the mean heat transfer coefficient of the working fluid can be calculated from Eqs. (4), (44), (45), (49) and (50).

3.1.1. Insulating cover plate

In case the cover plate has a very small thermal conductivity compared to that of the heat sink solid, the cover plate will behave as a perfect insulator, *i.e.*, $Q_2 = Q_{2a} \approx 0$. Criteria where this assumption is valid will be discussed in more detail in the next section. For an insulating cover plate,

$$Q_{base} = Q_b + Q_{fin} = Q_b + Q_1 \ [\mathrm{W/m}]. \tag{51}$$

Using Eq. (12) for a rectangular fin, the heat transfer rate at the fin base of the micro-channel unit cell can be written as

$$Q_{fin} = \sqrt{2hkW_s}(T_{w,b} - T_f)\tanh(mH_{ch}). \tag{52}$$

Applying the energy balance to the micro-channel heat sink shown in Fig. 1a yields

$$q''_{eff}(2H_{ch} + W_{ch}) = q''_{base}(W_s + W_{ch}) = Q_{fin} + Q_b. \tag{53}$$

3.2. Inverse trapezoidal cross-section

Similar to the solution procedure for the rectangular micro-channel unit cell, an energy balance for the inverse trapezoidal cross-section shown in Fig. 3b yields

$$Q_{base} = Q_b + Q_{fin} = Q_b + Q_1 + Q_2 \ [\mathrm{W/m}], \tag{54}$$

where

$$Q_b = hW_{ch,b}(T_{w,b} - T_f). \tag{55}$$

Using Eqs. (29) and (30) for a trapezoidal fin, the heat transfer rates at the fin base and the fin tip of the unit cell can be written, respectively, as

$$Q_{fin} = k(W_s + W_{ch,t} - W_{ch,b})m\sqrt{\frac{a}{H_{ch}+d}}\frac{\left[I_1\left(2m\sqrt{a(H_{ch}+d)}\right)K_0\left(2m\sqrt{ad}\right) + K_1\left(2m\sqrt{a(H_{ch}+d)}\right)I_0\left(2m\sqrt{ad}\right)\right](T_{w,b} - T_f) - \frac{(T_{w,t}-T_f)}{2m\sqrt{a(H_{ch}+d)}}}{I_0\left(2m\sqrt{a(H_{ch}+d)}\right)K_0\left(2m\sqrt{ad}\right) - K_0\left(2m\sqrt{a(H_{ch}+d)}\right)I_0\left(2m\sqrt{ad}\right)} \tag{56}$$

and

$$Q_2 = kW_s m\sqrt{\frac{a}{d}}\frac{\frac{(T_{w,b}-T_f)}{2m\sqrt{ad}} - \left[I_1\left(2m\sqrt{ad}\right)K_0(2m\sqrt{a(H_{ch}+d)}) + K_1\left(2m\sqrt{ad}\right)I_0(2m\sqrt{a(H_{ch}+d)})\right](T_{w,t} - T_f)}{I_0\left(2m\sqrt{a(H_{ch}+d)}\right)K_0\left(2m\sqrt{ad}\right) - K_0\left(2m\sqrt{a(H_{ch}+d)}\right)I_0\left(2m\sqrt{ad}\right)}, \tag{57}$$

where

$$m = \sqrt{\frac{2h}{k(W_s + W_{ch,t} - W_{ch,b})}}, d = \frac{W_s H_{ch}}{W_{ch,t} - W_{ch,b}} \quad \text{and}$$
$$a = \sqrt{\frac{1}{4}(W_s + W_{ch,t} - W_{ch,b})^2 + \left(H_{ch} + \frac{W_s H_{ch}}{W_{ch,t} - W_{ch,b}}\right)^2}. \tag{58}$$

An energy balance for the cover plate yields

$$Q_{2a} = hW_{ch,t}(T_{w,t} - T_f) = Q_2. \tag{59}$$

This procedure yields the following expression for fin tip temperature,

$$T_{w,t} = T_f + \frac{(T_{w,b} - T_f)}{2m\sqrt{ad}}\frac{1}{\xi_1}, \tag{60}$$

where

$$\xi_1 = I_1\left(2m\sqrt{ad}\right)K_0\left(2m\sqrt{a(H_{ch}+d)}\right) + K_1(2m\sqrt{ad})I_0\left(2m\sqrt{a(H_{ch}+d)}\right) + \frac{hW_{ch,t}}{kW_s m}\sqrt{\frac{d}{a}}\left[I_0(2m\sqrt{a(H_{ch}+d)})K_0\left(2m\sqrt{ad}\right) - K_0\left(2m\sqrt{a(H_{ch}+d)}\right)I_0\left(2m\sqrt{ad}\right)\right]. \tag{61}$$

Applying an energy balance to the micro-channel heat sink shown in Fig. 1 yields

$$q''_{eff}\left[W_{ch,t} + W_{ch,b} + \sqrt{4H_{ch}^2 + (W_{ch,t} - W_{ch,b})^2}\right] = q''_{base}(W_s + W_{ch,t}) = Q_{fin} + Q_b. \tag{62}$$

3.2.1. Insulating cover plate

For an insulating cover plate, the following energy balance is applied,

$$Q_{base} = Q_b + Q_{fin} = Q_b + Q_1 \ [\mathrm{W/m}]. \tag{63}$$

Using Eq. (24) for a trapezoidal fin, the heat transfer rate at the fin base of the micro-channel unit cell can be written as

$$Q_{fin} = k(W_s + W_{ch,t} - W_{ch,b})m\sqrt{\frac{a}{H_{ch}+d}} \times \frac{I_1\left(2m\sqrt{a(H_{ch}+d)}\right)K_1\left(2m\sqrt{ad}\right) - K_1\left(2m\sqrt{a(H_{ch}+d)}\right)I_1\left(2m\sqrt{ad}\right)}{I_0(2m\sqrt{a(H_{ch}+d)})K_1\left(2m\sqrt{ad}\right) + K_0\left(2m\sqrt{a(H_{ch}+d)}\right)I_1\left(2m\sqrt{ad}\right)} \times (T_{w,b} - T_f). \tag{64}$$

Applying an energy balance to the micro-channel heat sink shown in Fig. 1b yields

$$q''_{eff}[W_{ch,b}+\sqrt{4H_{ch}^2+(W_{ch,t}-W_{ch,b})^2}]=q''_{base}(W_s+W_{ch,t})=Q_{fin}+Q_b. \tag{65}$$

3.3. Triangular cross-section

As shown n Fig. 3c, energy conservation for a triangular cross-section can be expressed as

$$Q_{base}=Q_{fin}=Q_1+Q_2\ [\mathrm{W/m}]. \tag{66}$$

Using Eqs. (29) and (30) for the trapezoidal fin, the heat transfer rates at fin base and fin tip of triangular micro-channel unit cell shown in Fig. 3c can be written, respectively, as

$$Q_{fin}=k(W_s+W_{ch})m\sqrt{\frac{a}{H_{ch}+d}}\frac{\left[I_1\left(2m\sqrt{a(H_{ch}+d)}\right)K_0\left(2m\sqrt{ad}\right)+K_1\left(2m\sqrt{a(H_{ch}+d)}\right)I_0\left(2m\sqrt{ad}\right)\right](T_{w,b}-T_f)-\frac{(T_{w,t}-T_f)}{2m\sqrt{a(H_{ch}+d)}}}{I_0\left(2m\sqrt{a(H_{ch}+d)}\right)K_0\left(2m\sqrt{ad}\right)-K_0(2m\sqrt{a(H_{ch}+d)})I_0\left(2m\sqrt{ad}\right)} \tag{67}$$

and

$$Q_2=kW_sm\sqrt{\frac{a}{d}}\frac{\frac{(T_{w,b}-T_f)}{2m\sqrt{ad}}-\left[I_1\left(2m\sqrt{ad}\right)K_0\left(2m\sqrt{a(H_{ch}+d)}\right)+K_1\left(2m\sqrt{ad}\right)I_0\left(2m\sqrt{a(H_{ch}+d)}\right)\right](T_{w,t}-T_f)}{I_0\left(2m\sqrt{a(H_{ch}+d)}\right)K_0\left(2m\sqrt{ad}\right)-K_0\left(2m\sqrt{a(H_{ch}+d)}\right)I_0\left(2m\sqrt{ad}\right)}, \tag{68}$$

where

$$m=\sqrt{\frac{2h}{k(W_s+W_{ch})}},\quad d=\frac{W_sH_{ch}}{W_{ch}}\quad\text{and}$$
$$a=\sqrt{\frac{1}{4}(W_s+W_{ch})^2+\left(H_{ch}+\frac{W_sH_{ch}}{W_{ch}}.\right)^2}. \tag{69}$$

Applying an energy balance to the cover plate gives

$$Q_{2a}=hW_{ch}(T_{w,t}-T_f)=Q_2. \tag{70}$$

These relations yield the following expression for the fin tip temperature,

$$T_{w,t}=T_f+\frac{(T_{w,b}-T_f)}{2m\sqrt{ad}}\frac{1}{\xi_2}, \tag{71}$$

where

$$\xi_2=I_1\left(2m\sqrt{ad}\right)K_0\left(2m\sqrt{a(H_{ch}+d)}\right)+K_1\left(2m\sqrt{ad}\right)I_0\left(2m\sqrt{a(H_{ch}+d)}\right)+\frac{hW_{ch}}{kW_sm}\sqrt{\frac{d}{a}}\left[I_0\left(2m\sqrt{a(H_{ch}+d)}\right)K_0\left(2m\sqrt{ad}\right)-K_0\left(2m\sqrt{a(H_{ch}+d)}\right)I_0\left(2m\sqrt{ad}\right)\right]. \tag{72}$$

Applying an energy balance to the micro-channel heat sink shown in Fig. 1c yields

$$q''_{eff}\left[W_{ch}+\sqrt{4H_{ch}^2+W_{ch}^2}\right]=q''_{base}(W_s+W_{ch})=Q_{fin}. \tag{73}$$

3.3.1. Insulating cover plate

For an insulating cover plate,

$$Q_{base}=Q_{fin}=Q_1\ [\mathrm{W/m}]. \tag{74}$$

Using Eq. (24) for a trapezoidal fin, the heat transfer rates at the fin base of the unit cell can be written as

Applying an energy balance to the micro-channel heat sink shown in Fig. 1c yields

$$Q_{fin}=k(W_s+W_{ch})m\sqrt{\frac{a}{H_{ch}+d}}\frac{I_1\left(2m\sqrt{a(H_{ch}+d)}\right)K_1\left(2m\sqrt{ad}\right)-K_1\left(2m\sqrt{a(H_{ch}+d)}\right)I_1\left(2m\sqrt{ad}\right)}{I_0\left(2m\sqrt{a(H_{ch}+d)}\right)K_1\left(2m\sqrt{ad}\right)+K_0\left(2m\sqrt{a(H_{ch}+d)}\right)I_1\left(2m\sqrt{ad}\right)(T_{w,b}-T_f)}. \tag{75}$$

$$q''_{eff}\sqrt{4H_{ch}^2+W_{ch}^2}=q''_{base}(W_s+W_{ch})=Q_{fin}. \tag{76}$$

3.4. Trapezoidal cross-section

Following a solution procedure similar to that employed with the inverse trapezoidal cross-section, energy conservation for the trapezoidal micro-channel unit cell shown in Fig. 3d yields

$$q''_{eff}\left[W_{ch,t}+W_{ch,b}+\sqrt{4H_{ch}^2+(W_{ch,b}-W_{ch,t})^2}\right]=q''_{base}(W_s+W_{ch,b})=Q_{fin}+Q_b=kW_sm$$
$$\sqrt{\frac{a}{d}}\frac{\left[I_1\left(2m\sqrt{ad}\right)K_0\left(2m\sqrt{a(H_{ch}+d)}\right)+K_1\left(2m\sqrt{ad}\right)I_0(2m\sqrt{a}(H_{ch}+d))\right](T_{w,b}-T_f)-\frac{(T_{w,t}-T_f)}{2m\sqrt{ad}}}{I_0\left(2m\sqrt{a(H_{ch}+d)}\right)K_0\left(2m\sqrt{ad}\right)-K_0\left(2m\sqrt{a(H_{ch}+d)}\right)I_0\left(2m\sqrt{ad}\right)}+hW_{ch,b}(T_{w,b}-T_f), \quad (77)$$

where

$$m=\sqrt{\frac{2h}{kW_s}},\ d=\frac{W_sH_{ch}}{W_{ch,b}-W_{ch,t}} \quad \text{and}$$
$$a=\sqrt{\frac{W_s^2}{4}+\left(\frac{W_sH_{ch}}{W_{ch,b}-W_{ch,t}}\right)^2}. \quad (78)$$

This procedure yields the following expression for the fin tip temperature,

$$T_{w,t}=T_f+\frac{(T_{w,b}-T_f)}{2m\sqrt{a(H_{ch}+d)}}\frac{1}{\xi_3}, \quad (79)$$

where

$$\xi_3=I_1\left(2m\sqrt{a(H_{ch}+d)}\right)K_0\left(2m\sqrt{ad}\right)+K_1\left(2m\sqrt{a(H_{ch}+d)}\right)I_0\left(2m\sqrt{ad}\right)+\frac{hW_{ch,t}}{k(W_s+W_{ch,b}-W_{ch,t})m}\times\sqrt{\frac{H_{ch}+d}{a}}\left[I_0\left(2m\sqrt{a(H_{ch}+d)}\right)K_0\left(2m\sqrt{ad}\right)-K_0(2m\sqrt{a(H_{ch}+d)})I_0\left(2m\sqrt{ad}\right)\right]. \quad (80)$$

Table 1
Dimensions of micro-channels tested in the study of aspect ratio and fin spacing (total 30 cases, all dimensions are in μm).

	Rectangular	Inverse Trapezoidal	Triangular	Trapezoidal	Diamond	
H_{ch}	715 ($AR=H_{ch}/W_{ch}=4.3$), 168 ($AR=H_{ch}/W_{ch}=1.0$)					
W_s	42 ($W_s/W_{ch}=0.25$, $Bi=0.0027$)					
W_{ch}	$W_{ch,t}$	168	168	168	62	168
	$W_{ch,b}$		62		168	
H_{ch}	528 ($AR=H_{ch}/W_{ch}=4.3$), 124 ($AR=H_{ch}/W_{ch}=1.0$)					
W_s	86 ($W_s/W_{ch}=0.69$, $Bi=0.0055$)					
W_{ch}	$W_{ch,t}$	124	124	124	46	124
	$W_{ch,b}$		46		124	
H_{ch}	341 ($AR=H_{ch}/W_{ch}=4.3$), 80 ($AR=H_{ch}/W_{ch}=1.0$)					
W_s	130 ($W_s/W_{ch}=1.63$, $Bi=0.0084$)					
W_{ch}	$W_{ch,t}$	80	80	80	30	80
	$W_{ch,b}$		30		80	

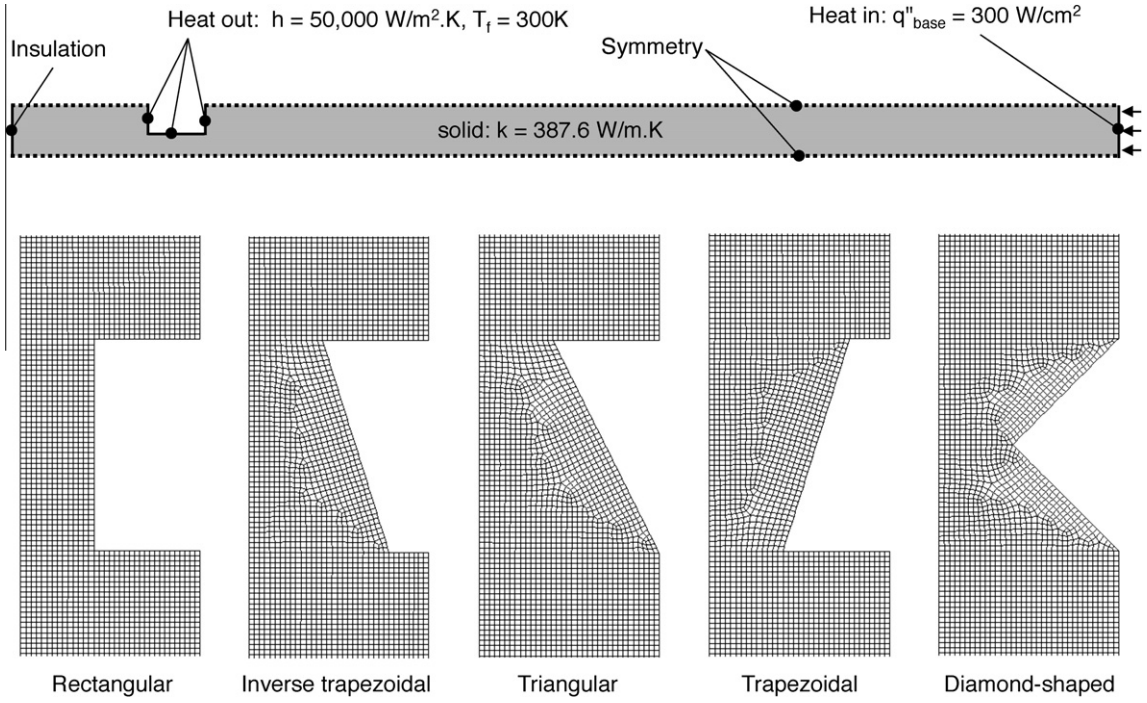

Fig. 4. Sample computational domain (shown turned 90°) of monolithic heat sink with rectangular cross-section and $H_{ch}=124$ μm, with magnification of micro-channel cross-sections for all five cross-sections with same channel height.

3.4.1. Insulating cover plate

Using Eq. (37) for an inverse trapezoidal fin, the heat transfer rate at the fin base of the unit cell can be written as

$$Q_{fin} = k(W_s + W_{ch})m\sqrt{\frac{a}{H_{ch}/2+d}}\frac{\left[I_1\left(2m\sqrt{a(H_{ch}/2+d)}\right)K_0\left(2m\sqrt{ad}\right)+K_1\left(2m\sqrt{a(H_{ch}/2+d)}\right)I_0\left(2m\sqrt{ad}\right)\right](T_{w,b}-T_f)-\frac{(T_2-T_f)}{2m\sqrt{a(H_{ch}/2+d)}}}{I_0\left(2m\sqrt{a(H_{ch}/2+d)}\right)K_0\left(2m\sqrt{ad}\right)-K_0(2m\sqrt{a(H_{ch}/2+d)})I_0\left(2m\sqrt{ad}\right)} \tag{83}$$

and

$$Q_2 = kW_s m\sqrt{\frac{a}{d}}\frac{\frac{(T_{w,b}-T_f)}{2m\sqrt{ad}}-\left[I_1\left(2m\sqrt{ad}\right)K_0\left(2m\sqrt{a(H_{ch}/2+d)}\right)+K_1\left(2m\sqrt{ad}\right)I_0\left(2m\sqrt{a(H_{ch}/2+d)}\right)\right](T_2-T_f)}{I_0(2m\sqrt{a(H_{ch}/2+d)})K_0\left(2m\sqrt{ad}\right)-K_0\left(2m\sqrt{a(H_{ch}/2+d)}\right)I_0\left(2m\sqrt{ad}\right)}, \tag{84}$$

$$\begin{aligned} Q_{fin} = {} & kW_s m\sqrt{\frac{a}{d}} \\ & \times\frac{I_1\left(2m\sqrt{a(H_{ch}+d)}\right)K_1\left(2m\sqrt{ad}\right)-K_1\left(2m\sqrt{a(H_{ch}+d)}\right)I_1\left(2m\sqrt{ad}\right)}{I_0\left(2m\sqrt{ad}\right)K_1\left(2m\sqrt{a(H_{ch}+d)}\right)+K_0\left(2m\sqrt{ad}\right)I_1\left(2m\sqrt{a(H_{ch}+d)}\right)} \\ & \times(T_{w,b}-T_f). \end{aligned} \tag{81}$$

Applying an energy balance to the micro-channel heat sink shown in Fig. 1d yields

$$\widehat{Q}_2 = kW_s(T_2-T_f)\hat{m}\sqrt{\frac{\hat{a}}{\hat{d}}}\frac{I_1(2\hat{m}\sqrt{\hat{a}(H_{ch}/2+\hat{d})})K_1(2\hat{m}\sqrt{\hat{a}\hat{d}})-K_1(2\hat{m}\sqrt{\hat{a}(H_{ch}/2+\hat{d})})I_1(2\hat{m}\sqrt{\hat{a}\hat{d}})}{I_0(2\hat{m}\sqrt{\hat{a}\hat{d}})K_1(2\hat{m}\sqrt{\hat{a}(H_{ch}/2+\hat{d})})+K_0(2\hat{m}\sqrt{\hat{a}\hat{d}})I_1(2\hat{m}\sqrt{\hat{a}(H_{ch}/2+\hat{d})})}, \tag{86}$$

$$\begin{aligned} & q''_{eff}\left[W_{ch,b}+\sqrt{4H_{ch}^2+(W_{ch,b}-W_{ch,t})^2}\right] = q''_{base}(W_s+W_{ch,b}) \\ & \quad = Q_{fin}+Q_b. \end{aligned} \tag{82}$$

3.5. Diamond-shaped cross-section

As shown in Fig. 3e, two separated trapezoidal regions may be considered for the analysis of a diamond-shaped micro-channel. For the lower trapezoidal region, the equations for the trapezoidal fin with boundary conditions of constant base temperature and prescribed tip temperature are applied. For the upper trapezoidal region, the equations for the inverse trapezoidal fin with boundary conditions of constant base temperature and adiabatic tip are applied, where Q_2 is used as the heat transfer rate at the fin base.

For the lower trapezoidal region, the heat transfer rate at fin base and fin tip are given, respectively, as

where

$$m = \sqrt{\frac{2h}{k(W_s+W_{ch})}},\ d = \frac{W_s H_{ch}}{2W_{ch}} \quad \text{and} \quad a = \sqrt{\frac{1}{4}(W_s+W_{ch})^2+\left(\frac{H_{ch}}{2}+\frac{W_s H_{ch}}{2W_{ch}}\right)^2}. \tag{85}$$

For the upper trapezoidal region, the heat transfer rate at the fin base is given by

where

$$\hat{m} = \sqrt{\frac{2h}{kW_s}},\quad \hat{d} = \frac{W_s H_{ch}}{2W_{ch}} \quad \text{and } \hat{a} = \sqrt{\frac{W_s^2}{4}+\left(\frac{W_s H_{ch}}{2W_{ch}}\right)^2}. \tag{87}$$

An energy balance at the interface between the upper and lower trapezoidal regions gives

$$Q_2 = \widehat{Q}_2. \tag{88}$$

This procedure yields the following expression for temperature at the interface between the two trapezoidal regions,

$$T_2 = T_f + \frac{(T_{w,b}-T_f)}{2m\sqrt{ad}}\frac{1}{\xi_4}, \tag{89}$$

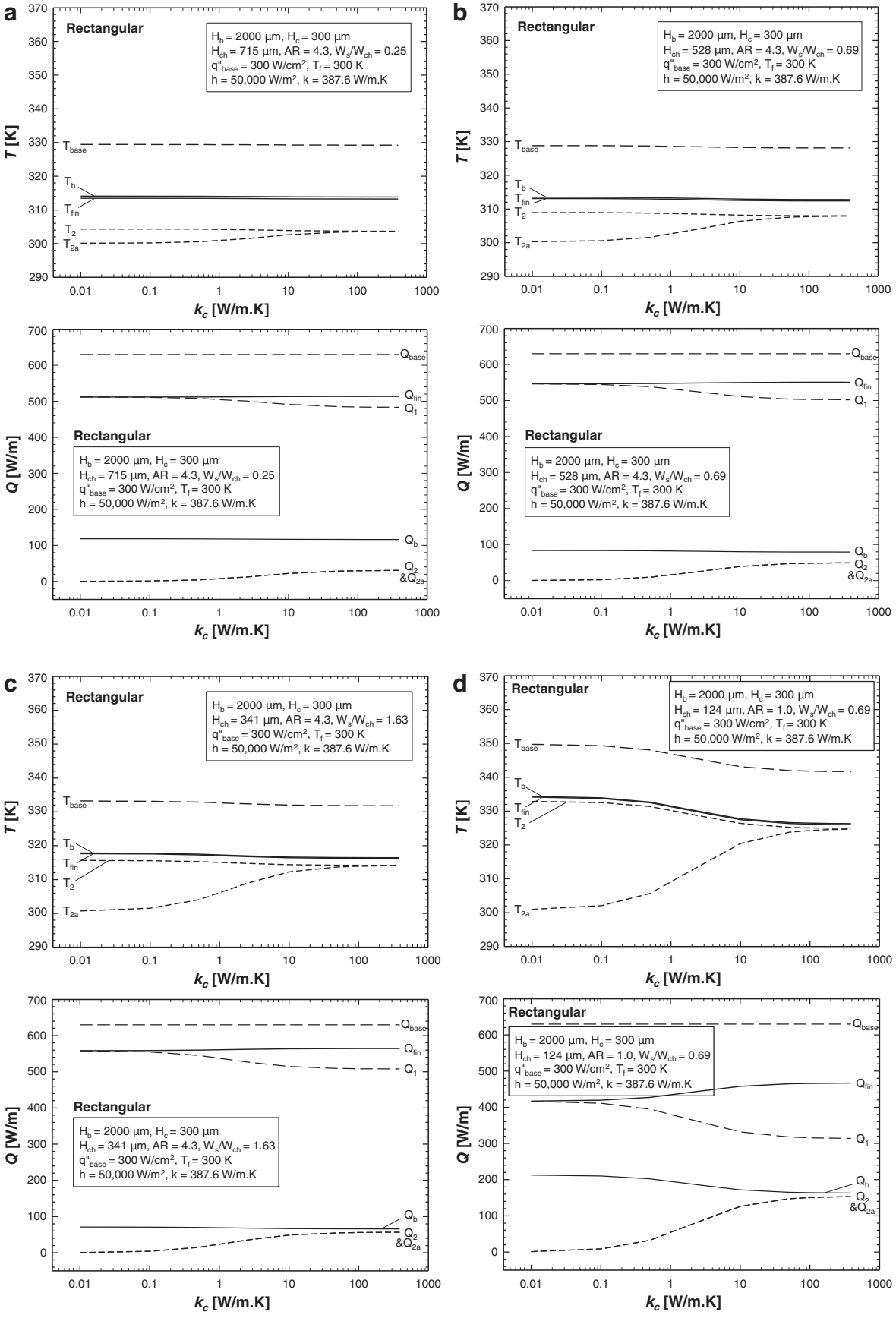

Fig. 5. Effects of thermal conductivity of cover plate for rectangular channel with (a) H_{ch} = 715 μm, (b) H_{ch} = 528 μm, (c) H_{ch} = 341 μm and (d) H_{ch} = 124 μm.

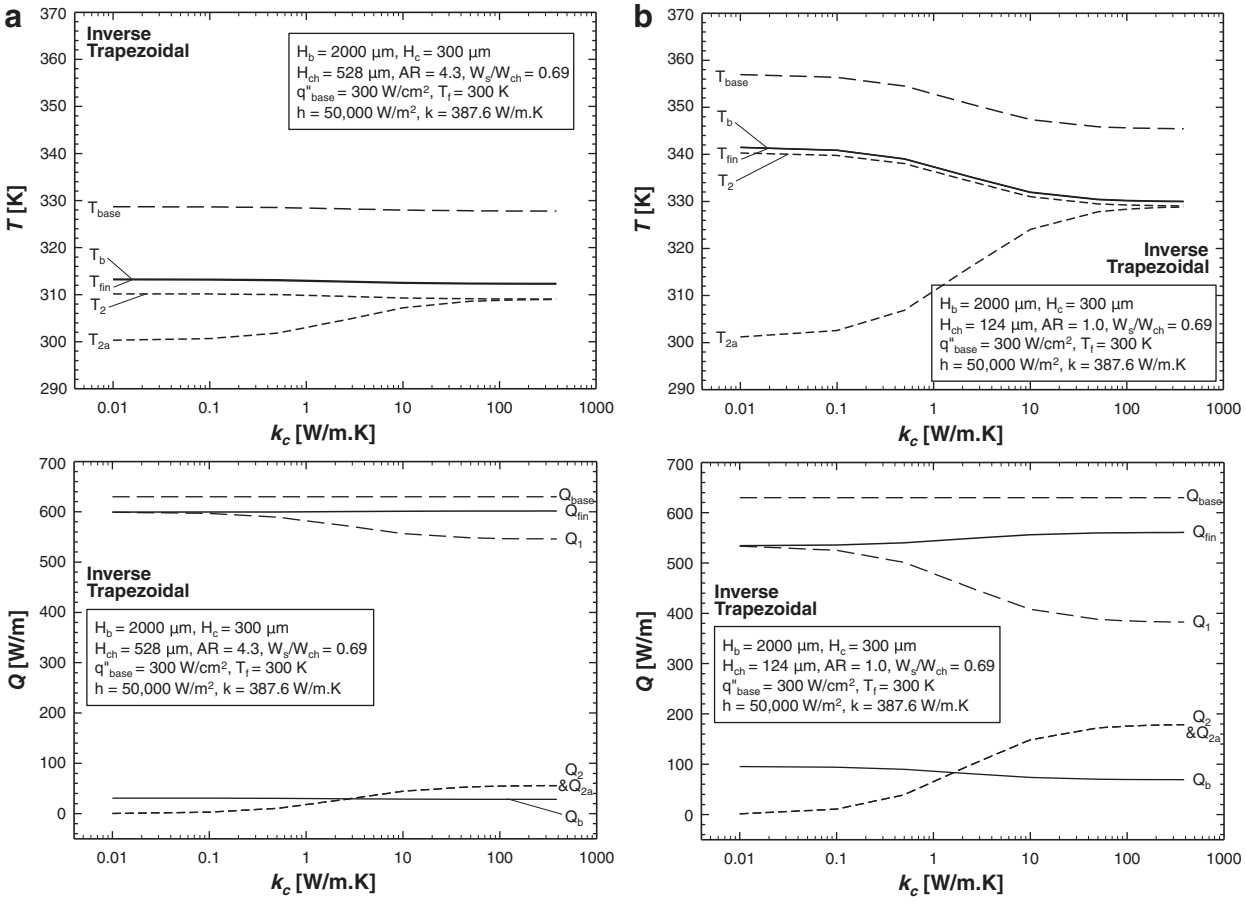

Fig. 6. Effects of thermal conductivity of cover plate for inverse trapezoidal channel with (a) H_{ch} = 528 μm and (b) H_{ch} = 124 μm.

where

$$\xi_4 = I_1\left(2m\sqrt{ad}\right)K_0\left(2m\sqrt{a(H_{ch}/2+d)}\right) + K_1\left(2m\sqrt{ad}\right)I_0\left(2m\sqrt{a(H_{ch}/2+d)}\right) + \frac{\hat{m}}{m}\sqrt{\frac{\hat{a}\hat{d}}{ad}}\frac{I_1\left(2\hat{m}\sqrt{\hat{a}(H_{ch}/2+\hat{d})}\right)K_1\left(2\hat{m}\sqrt{\hat{a}\hat{d}}\right) - K_1\left(2\hat{m}\sqrt{\hat{a}(H_{ch}/2+\hat{d})}\right)I_1\left(2\hat{m}\sqrt{\hat{a}\hat{d}}\right)}{I_0(2\hat{m}\sqrt{\hat{a}\hat{d}})K_1(2\hat{m}\sqrt{\hat{a}(H_{ch}/2+\hat{d})}) + K_0(2\hat{m}\sqrt{\hat{a}\hat{d}})I_1\left(2\hat{m}\sqrt{\hat{a}\left(H_{ch}/2+\hat{d}\right)}\right)} \times \left[I_0\left(2m\sqrt{a(H_{ch}/2+d)}\right)K_0\left(2m\sqrt{ad}\right) - K_0\left(2m\sqrt{a(H_{ch}/2+d)}\right)I_0\left(2m\sqrt{ad}\right)\right]. \quad (90)$$

Applying an energy balance to the micro-channel heat sink shown in Fig. 1e yields

$$q''_{eff}\sqrt{4H_{ch}^2+4W_{ch}^2} = q''_{base}(W_s+W_{ch}) = Q_{fin}. \quad (91)$$

4. Results

Table 1 shows the dimensions examined in the present study for the five micro-channel geometries. These dimensions are based on values from a parametric experimental study by Lee and Mudawar [17] involving rectangular micro-channels. Table 1 includes a total of 30 different cases that include channel aspect ratios of $AR = H_{ch}/W_{ch}$ = 4.3 and 1.0 and dimensionless fin spacings of W_s/W_{ch} = 0.25, 0.69, and 1.63. For validation of the analytical results, FLUENT 6.3 [18] was used to numerically solve the two-dimensional heat diffusion equation for each of the 30 cases. All simulations were conducted with copper as conducting solid using k = 387.6 W/m K, q''_{base} = 300 W/cm$_2$, h = 50,000 W/m^2 K, T_f = 300 K, H_b = 2000 μm, and H_c = 300 μm [17]. A convergence criterion of 10^{-11} was applied to the residuals of the energy equation. The two-dimensional meshes were created using GAMBIT 2.2 software [19]. Fig. 4 shows sample computational domains of the monolithic heat sink for H_{ch} = 124 μm. Grid independence was examined using two grid systems with 29,000 and 86,000 cells for rectangular channel with H_{ch} = 124 μm, which showed nearly identical temperature

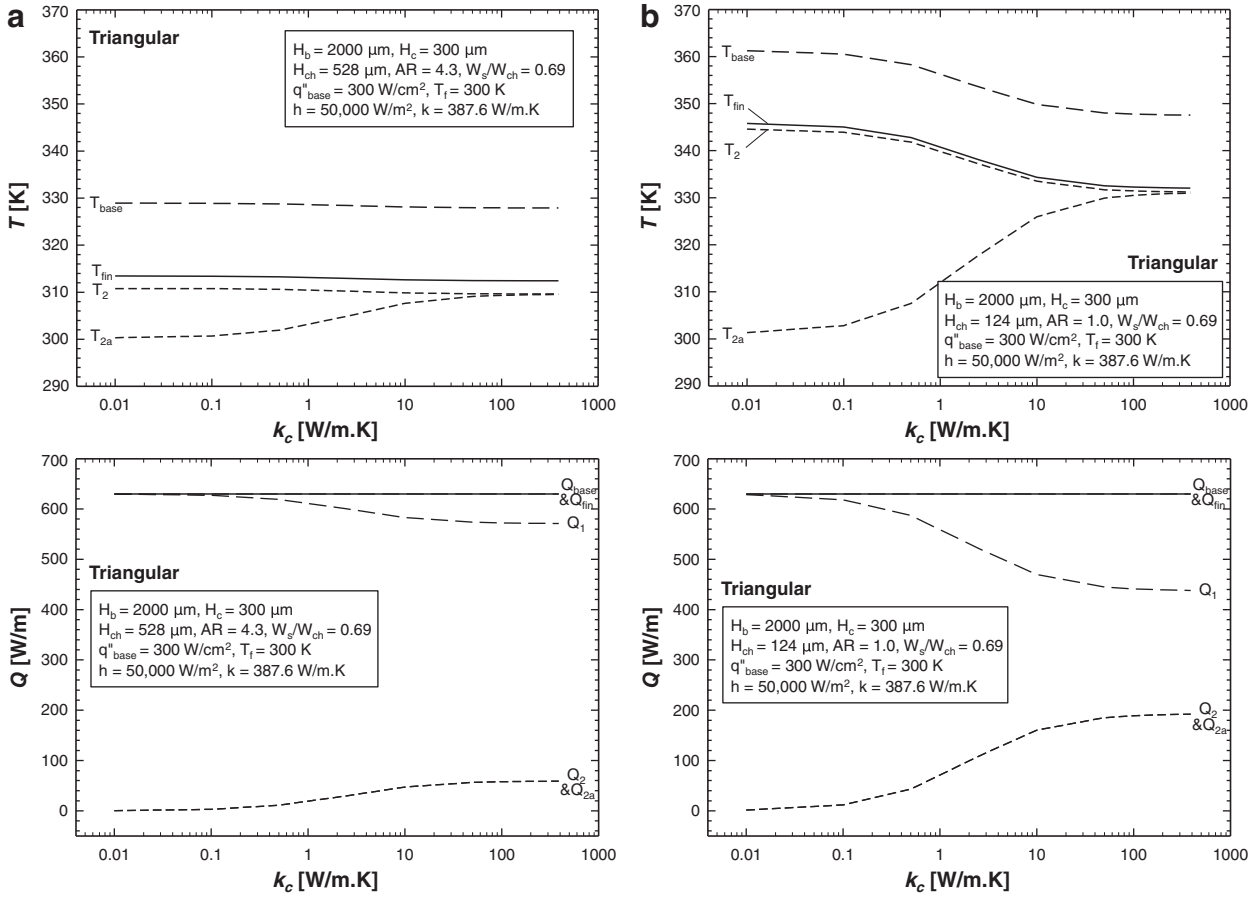

Fig. 7. Effects of thermal conductivity of cover plate for triangular channel with (a) H_{ch} = 528 μm and (b) H_{ch} = 124 μm.

distributions with differences in the area-averaged temperature and heat transfer rate at the fin base of less than 0.01%. For calculation efficiency, the grid system with 29,000 cells was used for all the simulations. For non-rectangular channels, meshes were generated with the same grid aspect ratio of the rectangular channel.

4.1. Effects of micro-channel aspect ratio and spacing

In order to examine the effects of thermal conductivity of cover plate, as well as various geometries, the area-averaged temperatures and heat transfer rates for H_{ch} = 528, 124, 715, and 341 μm were obtained from numerical simulations as shown in Figs. 5–8. The same input values of $q"_{base}$ = 300 W/cm^2, h = 50,000 W/m^2 K, and T_f = 300 K were used for all numerical simulations, and the temperatures and heat transfer rates represented are area-averaged values across the corresponding planes indicated in Fig. 3. In the case of $k_c = k$ = 387.6 (monolithic heat sink), Figs. 5–8 show the rectangular micro-channel produces lower T_2 and T_{fin}values compared to the other channel geometries. Conversely, the diamond channel produces higher T_2 and T_{tip}values, as indicated in Table 2. Moreover, comparing Figs. 5b and d, 6a and b, 7a and b and 8a and b, show T_2 and T_{fin} values are much lower for high AR channels than those for lower AR. For k_c = 387.6 and AR = 4.3, Fig. 5a–c show channels with the smallest fin spacing of W_s/W_{ch} = 0.25 produce much lower T_2 and T_{2a} values compared to those with larger spacings, W_s/W_{ch} = 0.69 and 1.63. Although relatively limited in parametric range, the present two-dimensional simulations suggest a rectangular micro-channel with a high aspect ratio and small fin spacing provides the best overall thermal performance compared to the other cross-sectional geometries based on the assumptions provided in Sections 2 and 3.

4.2. Effects of thermal conductivity of cover plate

For all micro-channel geometries, the two-dimensional simulations yield T_{fin} values that are nearly identical to those of T_b, which validates the second assumption adopted in the present analytical heat sink models. Figs. 5–8 show that T_{2a} approaches T_2 with increasing thermal conductivity of the cover plate, which validates the third assumption of the present analytical heat sink models for fairly to highly conducting cover plates. On the other hand, in case of a cover plate with very low thermal conductivity, Q_2 (which is equal to Q_{2a}) becomes negligible and $Q_1 \sim Q_{fin}$; *i.e.*, the cover plate behaves as perfectly insulating.

4.3. Effects of biot number

Fig. 9 shows the percent differences in heat transfer rate at the fin base, Q_{fin}, between the two-dimensional numerical results and present analytical solutions for AR = 4.3 and 1.0, W_s/W_{ch} = 0.69, and Bi ranging from 0.0055 to 0.2. Fig. 9 shows that for Bi < 0.2, the rectangular and trapezoidal channels for both aspect ratios yield higher differences between numerical and analytical results compared to the other channel geometries. It should be noted that the temperature difference between the fin base and the micro-channel bottom wall increases with increasing Biot number. Therefore, the second assumption adopted in the present micro-channel analytical heat sink models is not valid for high Bi values. Fig. 9

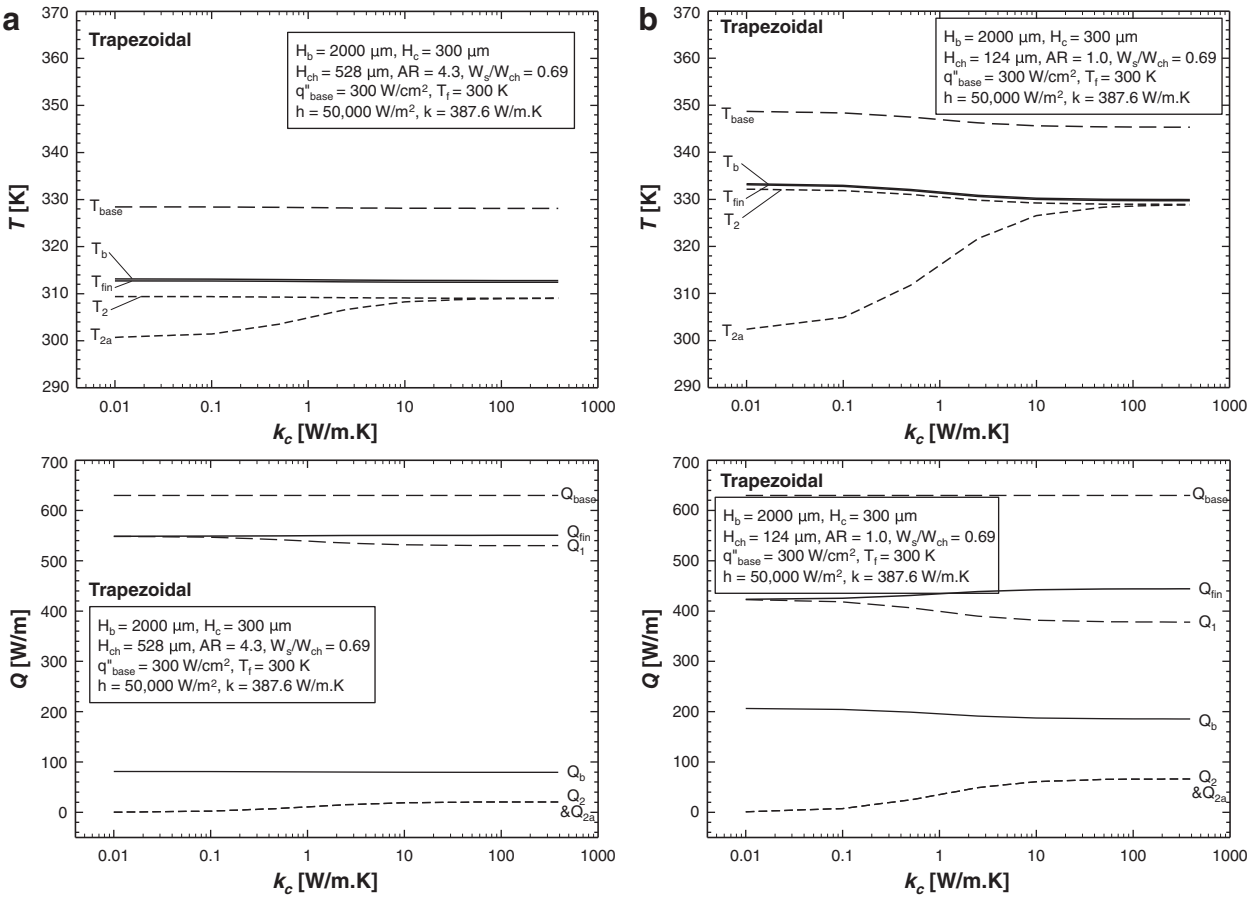

Fig. 8. Effects of thermal conductivity of cover plate for trapezoidal channel with (a) H_{ch} = 528 μm and (b) H_{ch} = 124 μm.

Table 2
Comparison of 2D numerical (area-averaged) and 1D analytical results for AR = 4.3, W_s/W_{ch} = 0.69 and $k_c = k$.

	Units	Rectangular			Inverse trapezoidal			Triangular			Trapezoidal			Diamond-shaped		
		Num.	Anal.	%Diff.	Num.	Anal.	%Diff.	Num.	Anal.	%Diff.	Num.	Anal.	%Diff.	Num.	Anal.	%Diff.
T_{base}	K	328.10	–		327.77	–		327.90	–		328.12	–		328.99	–	
T_{fin}	K	312.40	312.62	0.07	312.26	312.29	0.01	312.42	312.42	0.00	312.42	312.64	0.07	313.52	313.51	0.00
T_b	K	312.78		−0.05	312.41		−0.04	–			312.80		−0.05	–		
T_2	K	307.95	308.09	0.05	309.05	309.06	0.00	309.60	309.57	−0.01	309.12	309.19	0.02	311.40	311.39	0.00
T_{2a}, or T_{tip} for diamond	K	307.89		0.06	308.98		0.03	309.51		0.02	308.98		0.07	310.55	310.57	0.01
Q_b	W/m	79.28	78.24	−1.31	28.54	28.27	−0.95	–			79.38	78.37	−1.27	–		
Q_2	W/m	48.88	50.14	2.58	55.66	56.17	0.92	58.90	59.33	0.73	20.56	21.13	2.77	291.40	292.97	0.54
Q_{fin}	W/m	550.62	561.63	2.00	601.36	603.76	0.40	630.00	630.76	0.12	550.48	562.59	2.20	630.00	631.12	0.18

%Diff. = $(T_A - T_N)/T_N \times 100$ [%] or $(Q_A - Q_N)/Q_N \times 100$ [%].

shows that differences between the analytical and numerical results become appreciable only for fairly high Bi values that are beyond the range of interest for practical electronic cooling heat applications.

4.4. Assessment of overall accuracy of analytical models

To assess the accuracy of the analytical models for realistic heat sink geometries, values of the percent differences in the temperatures and the heat transfer rates for W_s/W_{ch} = 0.69, AR = 4.3 and Bi = 0.0055 are provided in Table 2. Very good agreement is realized between the present analytical model predictions and the two-dimensional numerical simulations, with maximum differences in temperature and heat transfer rate of 0.07% and 2.77%, respectively. The analytical models for the inverse trapezoidal, triangular, and diamond-shaped micro-channels show better predictions than for the rectangular and trapezoidal micro-channels.

Table 3 summarizes percent differences in Q_{fin} between analytical and numerical predictions for all 60 cases (30 cases indicated in Table 1 repeated for k_c = 0 and $k_c = k$), which feature the following Bi values: Bi = 0.0027 for H_{ch} = 715 and 168 μm, Bi = 0.0055 for H_{ch} = 528 and 124 μm, and Bi = 0.0084 for H_{ch} = 341 and 80 μm. The percent difference increases with decreasing fin spacing (W_s/W_{ch}) and increasing aspect ratio. Overall, the highest percent difference in heat transfer rate is 4.65%, which corresponds to the trapezoidal case with H_{ch} = 715 μm and $k_c = k$.

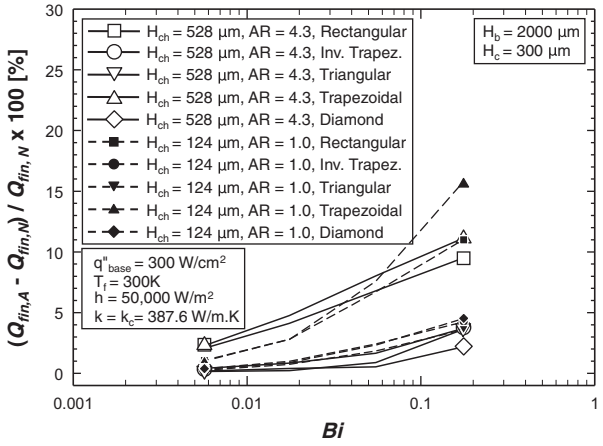

Fig. 9. Variation of percent difference between analytical and two-dimensional numerical results with Biot number for $W_s/W_{ch} = 0.69$.

Table 3
Percent difference in heat transfer rate between 2D numerical (area-averaged) and 1D analytical results.

H_{ch} (μm)		$(Q_{fin,A} - Q_{fin,N})/Q_{fin,N} \times 100$ (%)				
		Rectangular	Inverse trapezoidal	Triangular	Trapezoidal	Diamond
715	$k_c = 0$	3.72	0.53	−0.01	4.55	–
	$k_c = k$	3.78	0.58	0.05	4.65	0.25
168	$k_c = 0$	1.46	0.15	0.00	2.00	–
	$k_c = k$	2.53	0.55	0.37	2.36	0.57
528	$k_c = 0$	1.80	0.32	0.07	2.14	–
	$k_c = k$	2.00	0.39	0.15	2.21	0.18
124	$k_c = 0$	0.50	0.12	0.10	0.81	-
	$k_c = k$	1.01	0.36	0.24	0.96	0.30
341	$k_c = 0$	0.70	0.24	0.17	0.84	–
	$k_c = k$	0.76	0.25	0.23	0.81	0.26
80	$k_c = 0$	0.25	0.17	0.18	0.44	–
	$k_c = k$	0.42	0.27	0.23	0.45	0.25

5. Conclusions

This study examined heat diffusion effects in micro-channel heat sinks found in electronic cooling applications. Analytical models were constructed for heat sinks with rectangular, inverse trapezoidal, triangular, trapezoidal, and diamond-shaped micro-channels. Solutions were presented for both monolithic heat sinks as well as heat sinks with perfectly insulating cover plates. The analytical results were compared to two-dimensional numerical simulations for different micro-channel aspect ratios, fin spacings and Biot numbers. Key findings from the study can be summarized as follows:

(1) A systematic analytical methodology was developed for heat diffusion in the heat sinks which enables the determination of effective heat flux along the heated portion of the micro-channel and the mean wall temperature.

(2) Overall, a rectangular micro-channel with a high aspect ratio and small fin spacing provides the best overall thermal performance compared to the other cross-sectional geometries based on the assumptions provided in Sections 2 and 3.

(3) The analytical models for the inverse trapezoidal, triangular, and diamond-shaped micro-channels show better predictions than for the rectangular and trapezoidal micro-channels. Nonetheless, a maximum percent difference in heat transfer rate between the analytical and numerical results for 60 cases of practical interest of only 4.65% proves the analytical models are very accurate and effective tools for the design and thermal resistance prediction of micro-channel heat sinks found in electronic cooling applications.

Acknowledgement

The authors are grateful for the support of the Office of Naval Research (ONR) for this study.

References

[1] Y. Gan, J. Xu, S. Wang, Are the available boiling heat transfer coefficients suitable for silicon microchannel heat sinks?, Microfluids Nanofluids 4 (2008) 575–587.
[2] G. Hetsroni, A. Mosyak, E. Pogrebnyak, Z. Segal, Periodic boiling in parallel micro-channels at low vapor quality, Int. J. Multiphase Flow 32 (2006) 1141–1159.
[3] D. Klein, G. Hetsroni, A. Mosyak, Heat transfer characteristics of water and APG surfactant solution in a micro-channel heat sink, Int. J. Multiphase Flow 31 (2005) 393–415.
[4] G. Wang, P. Cheng, A.E. Bergles, Effects of inlet/outlet configurations on flow boiling instability in parallel microchannels, Int. J. Heat Mass Transfer 51 (2008) 2267–2281.
[5] H.Y. Wu, P. Cheng, Boiling instability in parallel silicon microchannels at different heat flux, Int. J. Heat Mass Transfer 47 (2004) 3631–3641.
[6] L. Jiang, M. Wong, Y. Zohar, Phase change in microchannel heat sinks with integrated temperature sensors, J. Microelectromech. Syst. 8 (1999) 358–365.
[7] W. Qu, I. Mudawar, Flow boiling heat transfer in two-phase micro-channel heat sinks-I. Experimental investigation and assessment of correlation methods, Int. J. Heat Mass Transfer 46 (2003) 2755–2771.
[8] J. Lee, I. Mudawar, Two-phase flow in high-heat-flux micro-channel heat sink for refrigeration cooling applications: Part II – heat transfer characteristics, Int. J. Heat Mass Transfer 48 (2005) 941–955.
[9] F.P. Incropera, D.P. Dewitt, Fundamentals of Heat and Mass Transfer, fifth ed., Wiley, New York, 2002.
[10] C. Cortés, L.I. Díez, A. Campo, Efficiency of composite fins of variable thickness, Int. J. Heat Mass Transfer 51 (2008) 2153–2166.
[11] P. Razelos, A critical review of extended surface heat transfer, Heat Transfer Eng. 24 (2003) 11–28.
[12] W.M. Murray, Heat dissipation through an annular disk or fin of uniform thickness, J. Appl. Mech. 60 (1938) A–78.
[13] K.A. Gardner, Efficiency of extended surface, Trans. ASME 67 (1945) 621–631.
[14] A.D. Kraus, A. Aziz, J. Welty, Extented Surface Heat Transfer, Wiley, New York, 2001.
[15] A. Bejan, A.D. Kraus, Heat Transfer Handbook, Wiley, New York, 2003.
[16] D.R. Harper, W.B. Brown, Mathematical equations for heat conduction in the fins of air-cooled engines, National Advisory Committee for Aeronautics, Report no. 158, 1922.
[17] J. Lee, I. Mudawar, Fluid flow and heat transfer characteristics of low temperature two-phase micro-channel heat sinks – Part 1: experimental methods and flow visualization results, Int. J. Heat Mass Transfer 51 (2008) 4315–4326.
[18] FLUENT Inc., Fluent 6 user's manual, Lebanon, NH, 2006.
[19] FLUENT Inc., Gambit 2 user's manual, Lebanon, NH, 2006.